Investigating Relationships between the Crystal Structure and ^{31}P Isotropic Chemical Shifts in Calcined Aluminophosphates

Daniel M. Dawson and Sharon E. Ashbrook*

School of Chemistry, EaStCHEM and Centre of Magnetic Resonance, University of St Andrews, North Haugh, St Andrews KY16 9ST, UK

*Author to whom correspondence should be addressed.

Telephone : +44 (0) 1334 463779

E-mail: *sema@st-andrews.ac.uk*

For submission to *J. Phys. Chem. C*

Abstract

Solid-state NMR spectra have historically been assigned using simple relationships between NMR parameters, *e.g.*, the isotropic chemical shift, and aspects of the local structure of the material in question, *e.g.*, bond angles or lengths. Density functional theory (DFT) calculations have effectively superseded these relationships in many cases, owing to the accuracy of the NMR parameters typically able to be calculated. However, the computational time required for DFT calculations may still be prohibitive, particularly for very large systems, where structure-spectrum relationships must still be used to interpret the NMR spectra. Here we show that, for calcined aluminophosphates (AlPOs), structure-spectrum relationships relying on either the mean P-O-Al angle or the mean P-O distance, both suggested in previous literature, provide a poor prediction of the ^{31}P isotropic shielding, σ_{iso}, calculated by DFT. However, a relationship dependent on both parameters yields predicted σ_{iso} in excellent agreement with DFT, with a mean error of ~1.6 ppm. The predictive ability of the relationship is not improved by introducing further parameters (many used in previous work) describing the local structure, suggesting that the two-parameter relationship is close to an optimum balance between accuracy and overparameterisation. The ability to predict accurately the outcome of DFT-level calculations will be of particular interest in cases where the actual calculations would be impractical or even impossible with current computational hardware, or where many such calculations are required quickly.

Keywords

Zeolites, solid-state NMR, density functional theory, local structure, spectral prediction, empirical relationships.

Introduction

Since their discovery in 1982,[1] aluminophosphate zeolites (AlPOs) have been a field of intense research, owing to their many potential applications in catalysis, medicine and gas storage.[2] As many of the elements present in AlPOs have NMR-active isotopes with favourable acquisition properties (most notably ^{31}P, ^{27}Al and, in many cases, ^{1}H and ^{19}F), solid-state NMR spectroscopy is often used to characterise these materials. Owing to its sensitivity to structure on the local (atomic) scale, the information provided is often complementary to the information able to be obtained by techniques based on Bragg diffraction. Solid-state NMR is particularly suited to the investigation of structural features such as disorder of framework-bound hydroxide and fluoride anions,[3-5] or of guest species within the pores,[6,7] as well as being sensitive to dynamic processes[8] – features of great importance for most applications of AlPOs. In many cases, AlPOs are substituted with isovalent or aliovalent cations (*e.g.*, Mg^{2+}, $Cr^{2/3+}$, Ga^{3+}, Si^{4+}, *etc.*,) to introduce catalytic properties to the framework.[2] The distribution of these species determines the position and behaviour of the active sites and the corresponding chemical and physical behaviour of the material, and solid-state NMR is ideally placed to investigate this typically non-periodic feature of the framework.[9-11]

One of the challenges of solid-state NMR spectroscopy is interpreting spectra in terms of the structural model of the material obtained by Bragg diffraction. While the symmetry of the material (*e.g.*, the number of crystallographically-distinct Al and P species in the framework) can readily be verified by the number of resonances present, it is not always clear which spectral resonance corresponds to which crystallographic species

when multiple resonances are present. In early work, this task of assignment was carried out using relatively simple relationships between structural features (*e.g.*, bond lengths or angles) and NMR parameters, most notably the relationship proposed by Müller *et al.*, between the ^{31}P isotropic shift, δ_{iso}, and the average P-O-Al bond angle, $\langle\theta_{POAl}\rangle$.[12] Since its publication, this relationship has been widely used to assign the ^{31}P NMR spectra of many phosphate materials, including templated[13-28] and calcined[27-30] AlPOs, AlPO-like clusters,[31,32] Si-doped AlPOs (SAPOs),[33,34] gallophosphates (GaPOs),[35,36] a zincophosphate (ZnPO)[37] and several other relevant structures.[20,38-40] The results of these assignments are plotted in Figure 1, and show a general trend of increasing δ_{iso} with decreasing $\langle\theta_{POT}\rangle$ (T = Al, Si, Ga, Zn, *etc.*,) for all classes of material included in the plot. However, it can be seen that the gradients, $d\delta_{iso}/d\langle\theta_{POAl}\rangle$, and y-intercepts are different for each class of material. Furthermore, there is a large scatter in the data, and all of the assignments are based on the relationship proposed by Müller *et al.*, meaning that they are inherently biased towards a trend for increasing δ_{iso} with decreasing $\langle\theta_{POAl}\rangle$. It should also be noted that the slope of the relationship of Müller *et al.* is in poor agreement with slopes observed for the different classes of materials in Figure 1, despite the basis of the spectral assignments in this relationship. The relationship between δ_{iso} and $\langle\theta_{POAl}\rangle$ reported by Kanehashi *et al.*,[41] also plotted in Figure 1, is in better general agreement with the overall dataset; perhaps a consequence of the fact that Müller *et al.* determined their relationship using a series of dense-phase $AlPO_4$ polymorphs (berlinite, cristobalite and tridymite), whereas Kanehashi *et al*. used data from two as-prepared AlPOs (VPI-5 and AlPO-14), which are structurally more similar to the other materials included on the plot. However, the degree of scatter of the experimental data from the lines representing both relationships is very high. These discrepancies may be partially explained by the fact that the values for both $\langle\theta_{POT}\rangle$ and δ_{iso}

are taken from experimental diffraction structures and NMR spectra, respectively, and so will vary in accuracy, depending on the precise experimental techniques and conditions used.

It is a well-known limitation of powder Bragg diffraction techniques that, while the unit cell parameters can be measured with a high degree of accuracy, and, for zeolites and related materials, the framework connectivity can also readily be determined, the precise positions of atoms are prone to larger errors. Therefore, one should exercise caution when comparing structural models derived in this way to the experimental NMR parameters, which are known to be extremely sensitive to the precise local structure. However, another possible explanation comes from the work of Campomar,[42] who suggested that the mean P-O bond length, $\langle r_{PO} \rangle$, influenced the ^{31}P δ_{iso} in a series of phosphates and, if the works of Müller *et al*., Kanehashi *et al*. and Campomar are to be believed, there must be at least two structural parameters influencing the chemical shifts of ^{31}P in metallophosphates. However, in recent years, the popularity of such simple relationships for spectral assignments in solids has dwindled as advances in computational hardware and electronic structure codes have enabled the calculation of extremely accurate NMR parameters for a range of complicated microporous materials.[43-49] This is particularly true for the periodic density functional theory (DFT) code, CASTEP,[50] which uses the gauge-including projector-augmented wavefunction (GIPAW)[51] approach. It has been shown that the GIPAW approach can be used to calculate accurate NMR parameters for many classes of materials,[44-49] providing that the structural model used as an input for the calculation of the NMR parameters is a reasonable representation of the true structure of the material.[29,48,49] DFT calculations based on the electronic structure of the system in question

may, then, be assumed to have superseded the use of the more primitive structure-spectrum relationships used in earlier assignments. However, DFT calculations are still computationally expensive, can require access to high-performance computing facilities and, while this approach can, in principle, be applied to very large systems (containing >200 atoms), the costs of calculating properties based on the electronic structures of systems much larger than this become prohibitive for most local computing facilities. While the NMR parameters of many AlPOs can, therefore, be calculated by DFT, those with either very large[52] or incommensurate[53,54] unit cells cannot be treated in this manner. In addition, many computational studies of disordered systems utilise a "supercell" approach to achieve a more realistic concentration of defects or substitutions,[55] which further challenges most computational facilities. Therefore, there still exists a need for an understanding of simple relationships between structural and spectral parameters, as many of the interesting and useful systems are currently at, or just beyond, the limit of current computational approaches and hardware.

Current structure-spectrum relationships typically relate a single structural feature to a single NMR parameter, and the outcome and general applicability of the relationships can vary widely.[56] Worthy of note are the two relationships (proposed by Müller *et al*. and Kanehashi *et al*.) between the ^{31}P δ_{iso} and $\langle\theta_{POAl}\rangle$, discussed above,[12,41] which show a markedly different dependence on the same parameter, as shown in Figure 1. In this work, we revisit the existing structure-spectrum relationships for ^{31}P δ_{iso} in AlPOs, using NMR parameters calculated using first-principles DFT calculations for known structures (in order to ensure that the NMR parameters arise from a known structure, rather than an assumed one, as would be the case in a purely experimental study). We begin by using a

"local cluster" approach to investigate in detail the relationship between ^{31}P δ_{iso} and $\langle\theta_{POAl}\rangle$ and $\langle r_{PO}\rangle$, demonstrating that both of these parameters must be taken into account when attempting to relate an NMR spectrum to structure. Based on these results, we then show that, when both $\langle\theta_{POAl}\rangle$ and $\langle r_{PO}\rangle$ are taken into account in the relationship, the DFT-level calculated δ_{iso} can be predicted from a given crystal structure of a calcined AlPO with a mean absolute error of ~1.6 ppm. Finally, we demonstrate that attempts to extend the relationship to include other local structural distortions may actually lead to overparameterisation, and that the simpler two-parameter relationship is likely to be more robust and generally applicable.

Experimental Details

DFT Calculations

Model cluster DFT calculations were carried out using GAUSSIAN 03 (revision D.01)[57] using the continuous set of gauge transformations (CSGT) method to calculate the NMR parameters. The B3LYP hybrid GGA functional was used, with the 6-311+G(2d,p) basis set employed for all atoms except the central P, for which the aug-pcS-2 basis set[58] was used. Prior to the calculation of the NMR parameters, the structures of the clusters were optimised to an energy minimum, with the parameters specified in the text constrained to their stated values. Calculations were carried out using a local cluster comprising four Intel Core i7-930 quad-core processors with 6 GB memory per core.

Periodic DFT calculations were performed using version 5.0 of the planewave CASTEP code,[50] which employs the GIPAW algorithm[51] to reconstruct the all-electron

wavefunction in the presence of a magnetic field. The generalised gradient approximation (GGA) PBE[59] functional was employed and core-valence interactions were described by ultrasoft pseudopotentials.[60] Wavefunctions were expanded as planewaves with a kinetic energy smaller than a cut-off energy of 60 Ry (816 eV). Integrals over the first Brillouin zone were performed using a Monkhorst-Pack grid with a k-point spacing of 0.04 $Å^{-1}$. Calculations were converged as far as possible with respect to both k-point spacing and cut-off energy. In some cases (see the Supporting Information), prior to the calculation of NMR parameters, the published crystal structures were optimised to an energy minimum using the same cut-off energy and k-point spacing as above, and with all atomic coordinates and unit cell parameters allowed to vary. Calculations were performed using the previous EaStCHEM Research Computing Facility, which consisted of 136 AMD Opteron 280 dual-core processors running at 2.4 GHz, partly connected by Infinipath high-speed interconnects.

Calculations generate the absolute shielding tensor, $\boldsymbol{\sigma}$, in the crystal frame. From the principal components of the symmetric part of the shielding tensor it is possible to generate the isotropic shielding $\sigma_{iso} = (1/3)\ \mathrm{Tr}\{\boldsymbol{\sigma}\}$. The isotropic chemical shift, δ_{iso}, is given (assuming $\sigma_{ref} << 1$), by $-(\sigma_{iso} - \sigma_{ref})$, where σ_{ref} is a reference shielding, here 279.28 ppm (for the CASTEP calculations), determined by comparing the calculated and experimental ^{31}P δ_{iso} of calcined AlPO-14.

Solid-State NMR

The solid-state ^{31}P MAS NMR spectrum of calcined AlPO-14 was recorded using a Bruker Avance III spectrometer, equipped with a 14.1 T wide-bore superconducting

magnet. The sample was packed in a 4 mm zirconia rotor and rotated at the magic angle at a rate of 14 kHz. The spectrum was recorded using a nutation frequency ($\omega_1/2\pi$) of ~100 kHz. Signal averaging was carried out for 4 transients with a recycle interval of 30 s. Experimental chemical shifts are reported relative to 85% H_3PO_4 using BPO_4 (δ = –29.6 ppm) as a secondary reference.

Linear Regression

Multivariate linear regression was carried out using MATLAB[61] routines described in further detail in the Supporting Information.

Results and Discussion

In order to investigate the influence of $\langle\theta_{POAl}\rangle$ and $\langle r_{PO}\rangle$ on σ_{iso}, several series of model clusters of the formula $[P(OAl(OH)_3)_4]^{3-}$, shown in Figure 2, were considered. The use of these model clusters enables $\langle\theta_{POAl}\rangle$ or $\langle r_{PO}\rangle$ to be varied systematically for the central atom, without having to take into account the longer-range structural constraints imposed by the extended framework structure of an AlPO. In the first set of clusters all P-O bond lengths and O-P-O bond angles were constrained to 1.52 Å and 109.47°, respectively, while $\langle\theta_{POAl}\rangle$ was varied according to Table 1. For each cluster, σ_{iso} for the central P atom was calculated with GAUSSIAN03[57] and, as shown in Figure 3(a), when only $\langle\theta_{POAl}\rangle$ is varied (series 1), there is a strong linear correlation (R^2 = 0.995) between σ_{iso} and $\langle\theta_{POAl}\rangle$ with $d\sigma_{iso}/d\langle\theta_{POAl}\rangle$ = 1.05 ppm per degree. For series 2 and 3, $\langle\theta_{POAl}\rangle$ was kept constant at 140° while the maximum and minimum θ_{POAl} ($\max(\theta_{POAl})$ and $\min(\theta_{POAl})$, respectively) and, hence, the standard deviation of θ_{POAl}, $\sigma(_{POAl})$, were varied. For series 2,

this was achieved by varying two of the angles, while the remaining two were fixed at 140°, whereas, in series 3, all four angles were varied, with two decreased and two increased, meaning that, for a given value of n, $\sigma(_{POAl})$ was larger in series 3 than in series 2. As can be seen in Figure 3(b), a difference is observed of up to –6.7 ppm (series 3, n = 7) in σ_{iso} relative to the corresponding point of series 1 (n = 7), in which $\langle\theta_{POAl}\rangle$ = 140° and $\sigma(_{POAl})$ = 0. This indicates that, as one might expect, the individual bond angles contribute to σ_{iso}, rather than just $\langle\theta_{POAl}\rangle$.

The calculations in series 4, 5, 6 and 7 provide further evidence that the individual P-O-Al angles, rather than just $\langle\theta_{POAl}\rangle$, contribute to σ_{iso}. In series 4, one angle was varied systematically, while the other three were adjusted so that $\langle\theta_{POAl}\rangle$ = 140°. In series 5 and 6, either max(θ_{POAl}) (series 5) or min(θ_{POAl}) (series 6) were fixed, one other angle was varied systematically and the other two angles were adjusted so that $\langle\theta_{POAl}\rangle$ = 140°. The calculated σ_{iso} for these three series is shown in Figure 3(b) and, as for series 2, it can be seen that $\sigma(_{POAl})$ contributes to σ_{iso} (here up to –5.8 ppm for series 4, n = 14). For series 7, one angle was varied systematically while the other three were fixed at 140°, so that both $\langle\theta_{POAl}\rangle$ and $\sigma(_{POAl})$ were varied systematically. As can be seen from Figure 3(a) there is a strong linear relationship between σ_{iso} and $\langle\theta_{POAl}\rangle$ for n ≤ 12 ($\langle\theta_{POAl}\rangle \leq 147.5°$, max($\theta_{POAl}$) = 170°) but, at higher $\langle\theta_{POAl}\rangle$ (*i.e.*, when max(θ_{POAl}) approaches 180° and $\sigma(_{POAl})$ approaches a maximum of 20°), σ_{iso} is lower than would be expected. In order to further investigate the contributions of $\langle\theta_{POAl}\rangle$ and $\sigma(_{POAl})$ to σ_{iso}, another series of $[P(OAl(OH)_3)_4]^{3-}$ clusters, series 8, was studied, with randomly-generated $\theta_{POAl(i)}$. From Figure 3(a), it can be seen that series 1 and 8 have a very similar relationship between σ_{iso} and $\langle\theta_{POAl}\rangle$. The line of best fit for series 1,

$$\sigma_{iso} = 1.0504\langle\theta_{POAl}\rangle + 174.45 \ , \quad (1)$$

is in excellent agreement with that for series 8,

$$\sigma_{iso} = 1.0601\langle\theta_{POAl}\rangle + 172.38 \ , \quad (2)$$

where σ_{iso} and the y intercept are in ppm, $\langle\theta_{POAl}\rangle$ is in degrees and the gradient is given in ppm per degree. This similarity, combined with the high correlation coefficients (R^2) of 0.995 for series 1, and 0.987 for series 8, suggests that, in more realistic cases, $\langle\theta_{POAl}\rangle$ is actually a good predictor for σ_{iso}, despite the variation in $\sigma(_{POAl})$ of between 8.23 and 23.70° for series 8. The results of series 1-8 appear to confirm the work of Müller *et al*. and Kanehashi *et al*., although it should be noted that the gradients in Equations 1 and 2 are ~1.1 ppm per degree: between the value determined by Müller *et al*. (0.51 ppm per degree) and Kanehashi *et al*. (1.25 ppm per degree), but closer to the latter. The discrepancies between the three studies are likely to arise from the more limited size of the two experimental datasets – as can be seen from Figure 1, selecting at random any three or four of the experimental data points could readily yield a wide range of gradients.

The results of series 1 and 8 (Figure 3(a)) suggest that the contribution to σ_{iso} from $\sigma(_{POAl})$ is minimal, compared to the contribution from $\langle\theta_{POAl}\rangle$. It is interesting to note that the change in σ_{iso} in series 2-7, relative to series 1 (n = 7) is always negative with increasing $\sigma(_{POAl})$, indicating that min(θ_{POAl}) may play a more important role than max(θ_{POAl}) in determining σ_{iso} (as a lower $\langle\theta_{POAl}\rangle$ leads to lower calculated σ_{iso}). However, as shown in

Figures 3(c and d), when all four bond angles are randomly generated, there is no clear relationship between σ_{iso} and max(θ_{POAl}) or min(θ_{POAl}). As can be seen from Figure 3(e), $\sigma(_{POAl})$ also does not appear to have a significant linear correlation with σ_{iso} for series 8.

In a second set of structures, the effect of $\langle r_{PO} \rangle$ – suggested by Campomar[42] to influence σ_{iso} – was investigated. For this set of clusters, all O-P-O and P-O-Al bond angles were constrained to 109.47 and 140°, respectively, and $\langle r_{PO} \rangle$ was varied systematically as given in Table 2 (series 9 -12). A further 20 clusters with randomly-generated bond lengths were also included (series 13). It can be seen from Figure 4(a) that, when only $\langle r_{PO} \rangle$ is allowed to vary and all other structural parameters are kept constant (series 9), σ_{iso} and $\langle r_{PO} \rangle$ are related by

$$\sigma_{iso} = -375.01\langle r_{PO} \rangle + 891.49 \ , \quad (3)$$

with $R^2 = 0.9876$, where σ_{iso} and the y intercept are in ppm, $\langle r_{PO} \rangle$ in Å and the gradient is given in ppm per Å. However, the correlation is significantly improved ($R^2 > 0.9999$) by assuming a quadratic function of $\langle r_{PO} \rangle$:

$$\sigma_{iso} = -1158.9\langle r_{PO} \rangle^2 + 3166.2\langle r_{PO} \rangle - 1812.5 \ . \quad (4)$$

In series 10 and 11, the maximum and minimum r_{PO} (max(r_{PO}) and min(r_{PO}), respectively) were varied while $\langle r_{PO} \rangle$ was kept constant at 1.52 Å, enabling investigation of the influence of the standard deviation of r_{PO}, $\sigma(r_{PO})$. In series 10, two of the bond lengths were varied, while the remaining two were fixed at 1.52 Å, whereas, in series 11, all four lengths were

varied, with two decreased and two increased, meaning that, for a given value of n, the standard deviation, $\sigma(r_{PO})$ was larger in series 10 than in series 11. Figure 4(b) shows that the difference in $\sigma(r_{PO})$ (of up to 0.058 Å for series 11, n = 5) led to a difference in σ_{iso} of just 0.18 ppm, relative to the structure with $\langle r_{PO} \rangle$ = 1.52 Å but $\sigma(r_{PO})$ = 0 (series 9, n = 8). This indicates that $\sigma(r_{PO})$ has limited influence on σ_{iso}, although it may be that the range of $\sigma(r_{PO})$ considered here was too small to observe effects that would be more apparent with a greater distribution of r_{PO}. For series 12, both $\langle r_{PO} \rangle$ and σ (r_{PO}) were varied, with one bond length systematically increased while the other three were always 1.52 Å. As can be seen in Figure 4(a), a good linear relationship between σ_{iso} and $\langle r_{PO} \rangle$ was observed,

$$\sigma_{iso} = -352.37\langle r_{PO} \rangle + 858.37 \ , \quad (5)$$

with R^2 = 0.9993, and a marginally stronger correlation (R^2 = 0.9999) for the quadratic relationship,

$$\sigma_{iso} = -1465.2\langle r_{PO} \rangle^2 + 4098.5\langle r_{PO} \rangle - 2521.6 \ . \quad (6)$$

The differences between the coefficients of Equations 4 and 6, may arise owing to the small, contribution from $\sigma(r_{PO})$ observed for series 10 and 11. However, as was observed for series 1-8, the effect of $\sigma(\theta_{POAl})$ appeared to be artificially enhanced when the bond angles were varied systematically, compared to the random variation of bond angles used for series 8. This can again be seen with series 13, containing clusters with four randomly-generated P-O bond lengths, for which the best linear agreement (R^2 = 0.9929) was

$$\sigma_{iso} = -314.27\langle r_{PO}\rangle + 800.44 \ , \quad (7)$$

while the quadratic relationship,

$$\sigma_{iso} = -1189.7\langle r_{PO}\rangle^2 + 3288.6\langle r_{PO}\rangle - 1906.3 \ , \quad (8)$$

yielded $R^2 > 0.9999$. It can be seen that the coefficients in Equation 8 are very similar to those of Equation 4, indicating that, when the P-O-Al bond angles are fixed, the quadratic relationship with $\langle r_{PO}\rangle$ dominates σ_{iso}, even in the presence of a non-zero $\sigma(r_{PO})$ (up to 0.057 Å for series 13) and, as can be seen from Figure 4(c), no significant correlation of σ_{iso} with $\sigma(r_{PO})$ is observed.

The model cluster studies discussed above suggest that both $\langle\theta_{POAl}\rangle$ and $\langle r_{PO}\rangle$ influence the calculated ^{31}P σ_{iso} (and, therefore, presumably the experimental δ_{iso}, which should have a –1 : 1 correspondence with σ_{iso}). This finding is relatively unsurprising when one considers that the nuclear shielding arises in part from the motion of electrons in orbitals near to the P nucleus, which will be affected by the extent of overlap of the electronic orbitals of P and O, which will depend on both the bond lengths and angles. Therefore, while the works of Müller *et al.*,[12] Kanehashi *et al.*[41] and Campomar[42] all have some validity, the relationships reported do not fully capture the relationship between the ^{31}P δ_{iso} and the structure of AlPOs, owing to their inherent assumption that the influence of a single structural parameter dominates.

To extend the results of the model cluster calculations to the periodic structures of

AlPOs where both $\langle\theta_{POAl}\rangle$ and $\langle r_{PO}\rangle$ may vary simultaneously, and essentially independently of each other, it is necessary to compare the ^{31}P δ_{iso} of a series of calcined AlPOs with their crystal structures. However, if conducted experimentally, such an approach would suffer from two major issues. Firstly, there are several unreliable crystal structures for calcined AlPOs in the literature, as demonstrated previously for AlPO-14, for which NMR parameters calculated for the published crystal structure did not agree well with experiment but, once the structure was optimised using DFT, the agreement was considerably better,[29,49] suggesting that the problem lay with the original structure rather than the approach itself. Consequently, the equivalence of a reported structure of a material and the structure of the material actually studied in the NMR experiment may not always be assumed. Secondly, given the existence of two conflicting chemical shift scales for ^{31}P,[56] differing by 1.6 ppm (*i.e.*, on the order of the shift differences expected to arise from changes in the local structure), and the fact that resonances may be broadened and overlapped in the ^{31}P NMR spectra of calcined AlPOs, the reported experimental chemical shifts cannot always be assumed to be accurate, or reported relative to the same reference point (and the reference point used is not always clear in the literature). Therefore, an alternative strategy was used to assess the relevance of the model cluster calculations above.

It has been shown that first-principles DFT calculations can be used to calculate (generally very accurate) NMR parameters from a given structural model (assuming the structural model is an accurate representation of the material in question).[43,44,48,49] The advantage of using theoretical rather than experimental data is that the NMR parameters obtained correspond exactly to the known structure, even if the structure and, hence,

calculated NMR parameters do not match those of any corresponding material. The NMR parameters were calculated for 42 structures of calcined AlPOs; 31 of which were taken from the literature and used without further optimisation and 11 that were subsequently optimised to an energy minimum prior to the calculation of NMR parameters. In addition, the structures of the dense $AlPO_4$ phases, quartz and cristobalite, were used without further optimisation, and the structures of these two dense phases, as well as that of a third dense phase, tridymite, were optimised and also included in the study. The published structure of tridymite[62] was not included itself, owing to the presence of 180° P-O-Al bond angles, which are unrealistic (arising from the average position of the O atoms determined by diffraction) and caused problems with some of the calculations discussed below. A full list of structures used appears in the Supporting Information.

The calculated σ_{iso} of the 159 crystallographically-distinct P species are plotted against $\langle\theta_{POAl}\rangle$ or $\langle r_{PO}\rangle$ in Figures 5(a and b), and it can be seen that the lines of best fit for each parameter do not adequately describe the data, with R^2 of 0.3315 for the relationship with $\langle\theta_{POAl}\rangle$ and 0.8501 for the relationship with $\langle r_{PO}\rangle$ and mean absolute errors (MAEs) of 7.1 and 4.2 ppm, respectively. The best-fit quadratic function of $\langle r_{PO}\rangle$, shown in Figure 5(b), is also not a good description of the data (R^2 = 0.8614, MAE = 3.9 ppm). Particularly poor agreement is observed for the P species arising from the structure of AlPO-5 reported by Ikeda *et al*.[63] (ICSD entry 88566), which contains unusually long P-O bonds, up to 1.682 Å. This is most noticeable in the plot in Figure 5(a), where these points are highlighted, and it is clear that the contribution to σ_{iso} from $\langle r_{PO}\rangle$ cannot be ignored. In Figure 5(b), it can be seen that the points from ICSD 88566 lie much closer to the trendlines for the rest of the dataset, when plotted against $\langle r_{PO}\rangle$ rather than against $\langle\theta_{POAl}\rangle$, as in Figure 5(a), although

there is still significant scatter in the rest of the dataset. It would appear, therefore, that σ_{iso} is dependent upon both $\langle\theta_{POAl}\rangle$ and $\langle r_{PO}\rangle$, although the latter contributes more significantly (typically over 90%). However, neither parameter on its own will be able to explain fully the value of σ_{iso}.

Multivariate linear regression (described in further detail in the Supporting Information) was carried out in order to determine the best fit of σ_{iso} to, simultaneously, a linear function of $\langle\theta_{POAl}\rangle$ and a quadratic function of $\langle r_{PO}\rangle$. In order to assess the validity of this function, the 159 P species were split into a training set (to which the function would be fitted) of 150 values, and a test set (against which the function would be validated) of nine values. The best-fit function for the training set was determined to be

$$\sigma_{iso}(\langle\theta_{POAl}\rangle,\langle r_{PO}\rangle) = 0.898\langle\theta_{POAl}\rangle - 1190\langle r_{PO}\rangle^2 + 3320\langle r_{PO}\rangle - 2120 \ , \quad (9)$$

where all coefficients are reported to 3 s.f. (higher precision is given in the Supporting Information). It should be noted that coefficients given in Equation 9 are very similar to those given in Equations 2 and 8, although the y intercepts are different (owing to the different values of reference shielding, σ_{ref}, required for the different computational codes used to generate the model cluster and periodic structure calculations). This, however, does confirm the validity of the model cluster approach as a tool for evaluating structure-spectrum relationships for periodic crystalline structures. The plots of the predicted $\sigma_{iso}(\langle\theta_{POAl}\rangle,\langle r_{PO}\rangle)$ against σ_{iso} calculated by CASTEP for the training and test sets are shown in Figure 5(c), and it can be seen that this relationship represents a vast improvement upon attempting to predict the ^{31}P σ_{iso} from either $\langle\theta_{POAl}\rangle$ or $\langle r_{PO}\rangle$ alone. For the training set, R^2 =

0.9746 and MAE = 1.60 ppm and, for the test set, R^2 = 0.9910 and MAE = 0.49 ppm. While the results for the test set appear better than those for the training set, the training set contains the structure of AlPO-5 reported by Ikeda *et al.*,[62] (ICSD 88566) to include the greatest range of σ_{iso} and $\langle r_{PO} \rangle$ possible. Therefore, the apparent improvement in the predictive power of the relationship for the test set may, perhaps, be attributed in part to the test set sampling a smaller number P species with more "normal" structural parameters that will be better described by the relationship. Interestingly, the largest deviation between the calculated σ_{iso} and $\sigma_{iso}(\langle \theta_{POAl} \rangle, \langle r_{PO} \rangle)$ is 9.95 ppm for P3 of AlPO-11[64] (ICSD entry 63664), indicated in orange in Figure 5(c). This species has a relatively short $\langle r_{PO} \rangle$ of 1.457 Å, as well as a relatively large $\langle \theta_{POAl} \rangle$ of 169.4° and, while these values do not represent the extremes of either $\langle r_{PO} \rangle$ or $\langle \theta_{POAl} \rangle$, their combination appears to have led to a large deviation between the calculated and predicted σ_{iso}. However, the MAE for this relationship is now of the same order of magnitude as the differences between the experimental chemical shifts of ^{31}P in most AlPOs, and its predictive power is good (*i.e.*, the relationship describes equally well the test and training sets). Therefore, this relationship is likely to be significantly more useful than any of the single-parameter relationships found in the literature.

Improving the Relationship

In the ^{31}P MAS NMR spectra of many calcined AlPOs, the shift difference between two resonances is small compared to the MAE of the relationship for σ_{iso} given in Equation 9. For example, in the ^{31}P NMR spectrum of calcined AlPO-14, shown in Figure 6(a), the δ_{iso} values for P2 and P4 (using the earlier assignment of Ashbrook *et al.*[29]) differ by just 0.7

ppm. Therefore, while it would be possible (as shown in Figures 6(b and c)) to assign the spectrum using either σ_{iso} calculated by CASTEP, which predicts a shift difference of 1.15 ppm for the optimised structure or by $\sigma_{iso}(\langle\theta_{POAl}\rangle,\langle r_{PO}\rangle)$ (predicted shift difference of 1.06 ppm), the assignment would perhaps require further experimental confirmation, such as heteronuclear correlation experiments. As such, it would be desirable to reduce the MAE and improve confidence in any assignments made on the basis of the local structure only. The most obvious way to achieve this would be to extend the number of parameters describing the local structure, as it would be naïve to assume that the full electronic structure of an AlPO, which ultimately gives rise to σ_{iso}, can adequately be described by two parameters – an average bond length and an average bond angle.

Various distortion parameters, described in more detail in the Supporting Information and summarised in Table 3, have been introduced in the literature in order to describe the coordination environment of a given species in terms of the deviation from either the mean or some "ideal" value of, *e.g.*, bond lengths or angles.[56,65-67] Here, the deviation of the bond lengths from the ideal and mean values was described by the longitudinal strain $|\alpha_{PO}|$, the standard deviation, $\sigma(r_{PO})$, and a deviation parameter, $\Delta(r_{PO})$, parameters, respectively. The O-P-O bond angles were described by their standard deviation, $\sigma(\theta_{OPO})$, and their deviation from ideality was characterised by the shear strain parameter, $|\Psi_{OPO}|$. For the P-O-Al angles, deviation from the mean was described by the standard deviation, $\sigma(\theta_{POAl})$, but as the P-O-Al bonds bridge two tetrahedra, it is not possible to define an "ideal" value (unlike the O-P-O angles, for which the ideal tetrahedral angle of 109.47° was used). The displacement of the P atom from the centre of the PO_4 tetrahedron, described by a displacement parameter, $|\mathbf{r}_{PO}|$, was also considered.

In order to assess the relevance of all parameters simultaneously, the multivariate linear regression procedure was modified to include feature selection, where parameters with an insignificant correlation with σ_{iso} were discarded and this linear regression with feature selection (LRFS) process (described in more detail in the Supporting Information) was repeated iteratively until only significant parameters remained. In addition to the parameters discussed above, the maximum, minimum and standard deviation of the P-O bond lengths, O-P-O and P-O-Al bond angles were considered. Next-nearest neighbour effects were taken into account by calculating the same distortion parameters for the (non-bonded) PAl_4 tetrahedron around P.

The predicted ^{31}P σ_{iso} as a function of the structural parameters considered here, σ_{iso}(structure), was determined by LRFS to be

$$\sigma_{iso}(\text{structure}) = 23\ \max(r_{PO}) - 47\ \min(r_{PO}) + 2300\ \langle r_{PO}\rangle - 850\ \langle r_{PO}\rangle^2 - 280\ \Delta(r_{PO}) - 39\ |\alpha_{PO}| + 0.14\ \min(\theta_{OPO}) + 1.7\ \langle\theta_{OPO}\rangle + 0.24\ \min(\theta_{POAl}) - 0.24\ \max(\theta_{POAl}) + 0.93\ \langle\theta_{POAl}\rangle + 0.44\ \sigma(\theta_{POAl}) - 57\ \min(r_{PAl}) + 23\ \max(r_{PAl}) + 720\ \langle r_{PAl}\rangle - 110\ \langle r_{PAl}\rangle^2 - 100\ \sigma(r_{PAl}) - 23\ |\alpha_{PAl}| + 0.17\ \min(\theta_{AlPAl}) - 0.15\ \max(\theta_{AlPAl}) + 1.8\ \sigma(\theta_{AlPAl}) - 7.4\ |\Psi_{AlPAl}| - 2600\ , \quad (10)$$

where all parameters are defined in the Supporting Information. All coefficients are reported to 2 s.f. (higher precision is given in the Supporting Information) and have units (or scaling factors, as appropriate) of ppm per Å (lengths, in Å), ppm per degree (angles, in °) and ppm (dimensionless distortion parameters, and the intercept), giving σ_{iso}(structure) in ppm. As shown in Figure 5(d), this relationship for σ_{iso}(structure) yields

generally good agreement for the training set (R^2 = 0.9947, MAE = 0.76 ppm) and the test set (R^2 = 0.9646, MAE = 1.10 ppm). However, the marginally improved agreement with the training set, at the expense of predictive ability for the test set, may be seen as evidence of overparameterisation (*i.e.,* the relationship describes in great detail small rounding or computing errors in the training set, rather than the more generally transferrable trends). Indeed, as shown in Figure 6(d), σ_{iso}(structure) yields a markedly poorer calculation of the ^{31}P σ_{iso} for the optimised structure of AlPO-14 than $\sigma_{iso}(\langle\theta_{POAl}\rangle,\langle r_{PO}\rangle)$, with a predicted separation between the P2 and P4 resonances of 4.57 ppm. Of course, as the agreement is better for the dataset as a whole, choosing another AlPO as an example would likely have given a different picture. However, given that there appears to be evidence of overparameterisation for σ_{iso}(structure), $\sigma_{iso}(\langle\theta_{POAl}\rangle,\langle r_{PO}\rangle)$, as given in Equation 9, would appear to represent a more sensible choice of structure-spectrum relationship; offering comparable accuracy and, apparently, more general transferability to the test set.

Conclusions and Further Work

In this work, it was shown that, for calcined AlPOs, very simple structure-spectrum relationships, relying on just one parameter, such as the mean P-O-Al bond angle, $\langle\theta_{POAl}\rangle$, or the mean P-O bond length, $\langle r_{PO}\rangle$, used in previous literature, provided a poor prediction of the (generally accurate) ^{31}P isotropic shielding, σ_{iso}, calculated by the periodic planewave density functional theory (DFT) code, CASTEP. However, a relationship dependent on both $\langle\theta_{POAl}\rangle$ and $\langle r_{PO}\rangle$ simultaneously was shown to yield predicted values of σ_{iso} in very good agreement with DFT-level calculations, with a MAE of ~1.6 ppm. It was demonstrated that the accuracy of the relationship could not be improved

significantly by the introduction of further parameters describing the local environment of the P atoms, suggesting that the simpler relationship is close to an optimum balance between accuracy and overparameterisation.

One disadvantage of the two-parameter relationship, $\sigma_{iso}(\langle\theta_{POAl}\rangle,\langle r_{PO}\rangle)$, is that, unlike the one-parameter models used in the literature, structural information cannot be inferred directly from the solid-state NMR spectrum, as a change in δ_{iso} could arise from a change in $\langle r_{PO}\rangle$ or $\langle\theta_{POAl}\rangle$ (although it is clear from the work reported here that such inferences based on the earlier relationships would not necessarily be correct if more than one structural parameter were changing between two different P species). However, as it is relatively fast to calculate $\sigma_{iso}(\langle\theta_{POAl}\rangle,\langle r_{PO}\rangle)$ for a given structure, it may be possible to use this relationship to "screen" a variety of possible structures to determine whether their calculated ^{31}P chemical shifts would be likely to match the experimental values. In addition, it may be possible to use experimental NMR parameters as a constraint for an iterative structural refinement procedure – one of the key aims of the "NMR crystallography" approach.

We are currently working on extending the principles outlined above to other porous materials related to calcined AlPOs. Initially, these will include "as-made" AlPOs, containing positively-charged structure-directing agents within the pores and chalge-balancing anions bound to the framework Al species. However, systems such as the ordered gallophosphates (GaPOs) and silicate zeolites, and disordered silicon- and metal-doped aluminophosphates (SAPOs and MAPOs) and aluminosilicate zeolites (where the introduction of dilute substituent atoms must typically be described by a large supercell)

are also natural extensions to the work. In addition, ^{31}P NMR has been shown to be an important investigative tool for many other phosphate-based systems, including glasses,[41,56,68] nuclear waste storage materials,[69] electrically-active phosphates[busman-holder] and catalysts[71-73] and it may be of interest to attempt to transfer the principles of structure-spectrum relationships discussed in this work to these systems.

As well as extending this work to other chemical systems, we are extending the LRFS approach outlined above to the calculation of the anisotropic ^{31}P shielding tensor, as well as NMR parameters for ^{27}Al and ^{17}O in calcined AlPOs. While it is unlikely that such simplistic relationships can truly rival DFT-level calculations for structures of a few hundred atoms, it is hoped that they will be able to provide insight into larger systems, for which DFT-level calculations are currently unfeasible (materials with very large unit cells, disordered supercells, *etc*.). One potential application of particular interest would be molecular dynamics (MD) calculations, in which NMR parameters may be determined for each one of the many tens of thousands of steps in the run, allowing time-averaged NMR parameters to be obtained for such systems. This is likely to be relevant for as-made AlPOs and related materials, where the presence of dynamic guest molecules within the pores can potentially lead to time-averaged NMR parameters for the framework nuclei, as well as for systems containing isolated PO_4^{3-} species, which can often isotropically reorient at finite temperatures. Of particular relevance is the recent demonstration by Hansen *et al*. of a similar approach to study the ^{31}P shielding tensors in large ensembles of phospholipids (vesicles and bilayers) using simple models to successfully calculate the NMR parameters for each step of an MD calculation.[74]

Acknowledgements

We would like to thank EPSRC (EP/E041825/1 and EP/J501542/1) for support and for the award of a studentship to DMD. Scott Sneddon is acknowledged for assistance in the preparation of this manuscript.

Supporting Information Available: Details of the linear regression with feature selection (LRFS) procedure, list of random bond lengths and angles used for the model cluster calculations, list of the literature structures of calcined AlPOs used, coefficients of equations 9 and 10 to higher precision, discussion of the distortion parameters used, and complete Reference 57. This material is available free of charge via the Internet at http://pubs.acs.org.

References

1. Wilson, S. T.; Lok, B. M.; Messina, C. A.; Cannan, T. R.; Flanigen, E. M. Aluminophosphate Molecular Sieves: A New Class of Microporous Crystalline Inorganic Solids. *J. Am. Chem. Soc.*, **1982**, *104*, 1146-1147.

2. Wright, P. A. *Microporous Framework Solids*; The Royal Society of Chemistry, Cambridge, UK, 2008.

3. Martineau, C.; Bouchevreau, B.; Tian, Z.; Lohmeier, S.-J.; Behrens, P.; Taulelle, F. Beyond the Limits of X-ray Powder Diffraction: Description of the Nonperiodic Subnetworks in Aluminophosphate-Cloverite by NMR Crystallography. *Chem. Mater.*, **2011**, *23*, 4799-4809.

4. Martineau, C.; Mellot-Draznieks, C.; Taulelle, F. NMR Crystallography of $AlPO_4$-CJ2: from the Topological Network to the Local (OH)/F Distribution. *Phys. Chem. Chem. Phys.*, **2011**, *13*, 18078-18087.

5. Seymour, V. R.; Eschenroeder, E. C. V.; Castro, M.; Wright, P. A.; Ashbrook, S. E. Application of NMR Crystallography to the Determination of the Mechanism of Charge-Balancing in Organocation-Templated AlPO STA-2. *Cryst. Eng. Comm.*, **2013**, *15*, 8668-8679.

6. Ashbrook, S. E.; Cutajar, M.; Griffin, J. M.; Lethbridge, Z. A. D.; Walton, R. I.; Wimperis, S. Transformation of AlPO-53 to JDF-2: Reversible Dehydration of a Templated Aluminophosphate Studied by MAS NMR and Diffraction. *J. Phys. Chem. C*, **2009**, *113*, 10780-10789.

7. Khimyak, Y. Z.; Klinowski, J. Solid-State NMR Studies of the Organic Template in Mesostructured Aluminophosphates. *Phys. Chem. Chem. Phys.*, **2001**, *3*. 616-626.

8. Antonijevic, S.; Ashbrook, S. E.; Biedasek, S.; Walton, R. I.; Wimperis, S.; Yang, H. Dynamics on the Microsecond Timescale in Microporous Aluminophosphate AlPO-14 as

Evidenced by ^{27}Al MQMAS and STMAS NMR Spectroscopy. *J. Am. Chem. Soc.* **2006**, *128*, 8054-8062.

9. Barrie, P. J.; Klinowski, J. Ordering in the Framework of a Magnesium Aluminophosphate Molecular Sieve. *J. Phys. Chem.*, **1989**, *93*, 5972-5974.

10. Mali, G.; Ristic, A.; Kaucic, V. ^{31}P NMR as a Tool for Studying Incorporation of Ni, Co, Fe, and Mn into Aluminophosphate Zeotypes. *J. Phys. Chem. B*, **2005**, *109*, 10711-10716.

11. Deroche, I.; Maurin, G.; Llewellyn, P. L.; Castro, M.; Wright, P. A. Silicon Distribution in SAPO Materials: A Computational Study of STA-7 Combined to ^{29}Si MAS NMR Spectroscopy. *Micropor. Mesopor. Mater.*, **2008**, 268-275.

12. Müller, D.; Jahn, E.; Ladwig, G.; Haubenreisser, U. High-Resolution Solid-State ^{27}Al and ^{31}P NMR: Correlation Between Chemical Shift and Mean Al-O-P Angle in $AlPO_4$ Polymorphs. *Chem. Phys. Lett.*, **1984**, *109*, 332-336.

13 Soulard, M.; Patarin, J.; Marler, B. Synthesis and Structure of Mu-10: a Novel Microporous Hydroxyaluminophosphate $(CH_3)_2NH_2 \cdot Al_3P_3O_{12}OH$ Closely Related to $AlPO_4$-EN3. *Solid State Sci.*, **1999**, *1*, 37-53.

14. Hartmann, M.; Prakash, A. M. Kevan, L. Multinuclear MAS NMR Study on the Microporous Aluminophosphates $AlPO_4$-41 and SAPO-41. *J. Chem. Soc. Faraday Transact.*, **1998**, *94*, 723-727.

15. He, H.; Klinowski, J. Solid-State NMR Studies of the Aluminophosphate Molecular Sieve AIPO4- 18. *J. Phys. Chem.*, **1993**, *97*, 10985-10388.

16. Logar, N. Z.; Mali, G.; Rajic N.; Jevtic, S.; Rangus, M.; Golobic, A.; Kaucic, V. Structure Investigation of Fluorinated Aluminophosphate ULM-3 Al Templated by 3-methylaminopropylamine. *J. Solid State Chem.*, **2010**, *183*, 1055-1062.

17. Byrne, P. J.; Warren, J. E.; Morris, R. E.; Ashbrook, S. E. Structure and NMR

Assignment in $AlPO_4$-15: A Combined Study by Diffraction, MAS NMR and First-Principles Calculations *Solid State Sci.*, **2009**, *11*, 1001-1006.

18. Fjellvåg, H.; Akporiaye, D. E.; Halvorsen, E. N.; Karlsson, A.; Kongshaug, K. O.; Lillerud, K. P. Crystal Structure and MAS-NMR Study of Rehydrated UiO-7. *Solid State Sci.*, **2001**, *3*, 603-611.

19. Paillaud, J. L.; Caullet, P.; Schreyeck, L.; Marler, B. Mu-13: A New $AlPO_4$ Prepared with 4,13-diaza-18-crown-6 as a Structuring Agent. *Micropor. Mesopor. Mater.*, **2001**, *42*, 177-189.

20. Tuel, A.; Gramlich, V.; Baerlocher, C. Synthesis, Crystal Structure and Characterisation of APDAO, a New Layered Aluminophosphate Templated by 1,8-diaminooctane Molecules. *Micropor. Mesopor. Mater.*, **2001**, *47,* 217-229.

21. Maeda, K.; Tuel, A.; Caldarelli, S.; Baerlocher, C. Synthesis, Structure Determination and Characterization of APDAB200, a New Aluminophosphate Prepared with 1,4-diaminobutane. *Micropor. Mesopor. Mater.*, **2000**, *39*, 465-476.

22. Kongshaug, K. O.; Fjellvåg, H.; Klewe, B.; Lillerud, K. P. Synthesis, Crystal Structure and Thermal Properties of the $AlPO_4$ Material UiO-12. *Micropor. Mesopor. Mater.*, **2000**, *39*, 333-339.

23. Canesson, L.; Arcon, I.; Caldarelli, S.; Tuel, A. Synthesis and Characterization of Cobalt-Containing Hydrated Aluminophosphate Molecular Sieves $CoAPO_4$-H3. *Micropor. Mesopor. Mater.*, **1998**, *26*, 117-131.

24. Fyfe, C. A.; Meyer zu Altenschildesche, H. M. Z.; Wong-Moon, K. C.; Grondey, H.; Chezeau, J. M. 1D and 2D Solid State NMR Investigations of the Framework Structure of as-Synthesized $AlPO_4$-14. *Solid State Nucl. Magn. Reson.*, **1997**, *9*, 97-106.

25. Li, H.-X.; Davis, M. E. Further Studies on Aluminophosphate Molecular Sieves Part 2.-VPI-5 and Related Aluminophosphate Materials. *J. Chem. Soc. Faraday Transact.*, **1993**, *89*,

957-964.

26. Engelhardt, G.; Veeman, W. Assignment of the ^{27}Al and ^{31}P NMR Spectra of the Aluminophosphate Molecular Sieve VPI-5. *J. Chem. Soc. Chem. Commun.*, **1993**, 622-623.

27. Li, H.-X.; Davis, M. E. Further Studies on Aluminophosphate Molecular Sieves Part 1.-$AlPO_4$-H2: A Hydrated Aluminophosphate Molecular Sieve. *J. Chem. Soc. Faraday Transact.*, **1993**, *89*, 951-965.

28. Akporiaye, D. E.; Fjellvåg, H.; Halvorsen, E. N.; Hustveit, J.; Karlsson, A.; Lillerud, K. P. UiO-7: A New Aluminophosphate Phase Solved by Simulated Annealing and High-Resolution Powder Diffraction. *J. Phys. Chem.*, **1996**, *100*, 16641-16646.

29. Ashbrook, S. E.; Cutajar, M.; Pickard, C. J.; Walton, R. I.; Wimperis, S. Structure and NMR Assignment in Calcined and As-Synthesized Forms of AlPO-14: a Combined Study by First-Principles Calculations and High-Resolution ^{27}Al–^{31}P MAS NMR Correlation. *Phys. Chem. Chem. Phys.*, **2008**, *10*, 5754-5764.

30. Seymour, V. R. *PhD. Thesis*; University of St Andrews, 2013.

31. Pinkas, J.; Löbl, J.; Dastych, D.; Necas, M.; Roesky, H. W. Adamantane-Like Aluminum Amide-Phosphate from Alumazene. *Inorg. Chem.*, **2002**, *41*, 6914-6918.

32 Yang, Y.; Pinkas, J.; Schafer, M.; Roesky, H. W. Molecular Model for Aluminophosphates Containing Fluoride as a Structure-Directing and Mineralizing Agent. *Angew. Chem. Int. Ed.*, **1998**, *37*, 2650-2653.

33. Yan, Z.; Chen, B.; Huang, Y. A Solid-State NMR Study of the Formation of Molecular Sieve SAPO-34. *Solid State Nucl. Magn. Reson.*, **2009**, *35*, 49-60.

34. Herreros, B.; Klinowski, J. Isomorphous Replacement of Al by Si in the Framework of $AlPO_4$-5 Using $(NH_4)_2SiF_6$. *J. Phys. Chem.*, **1995**, *99*, 9514-9518.

35. Beitone, L.; Marrot, J.; Loiseau, T.; Ferey, G.; Henry, M.; Huguenard, C.; Gansmuller,

A.; Taulelle, F. MIL-50, an Open-Framework GaPO with a Periodic Pattern of Small Water Ponds and Dry Rubidium Atoms: a Combined XRD, NMR, and Computational Study. *J. Am. Chem. Soc.*, **2003**, *125*, 1912-1922.

36. Amri, M.; Ashbrook, S. E.; Dawson, D. M.; Griffin, J. M.; Walton, R. I.; Wimperis, S. A Multinuclear Solid-State NMR Study of Templated and Calcined Chabazite-Type GaPO-34 *J. Phys. Chem. C*, **2012**, *116*, 15048-15057.

37. Kongshaug, K. O.; Fjellvåg, H.; Lillerud, K. P. The Synthesis and Crystal Structure of a New Open-Framework Zincophosphate UiO-17. *J. Mater. Chem.*, **1999**, *9*, 3119-3123.

38. Akporiaye, D. E.; Andersen, A.; Dahl, I. M.; Mostad, H. B.; Wendelbo, R. Synthesis and Characterization of the Magnesium Silicoaluminophosphates MAPSO-43 and MAPSO-39. *J. Phys. Chem.*, **1995**, *99*, 14142-14148.

39. Tuel, A.; Lorentz, C.; Gramlich, V.; Baerlocher, C. Synthesis, Characterization and Structure Determination of Two Isotypes of a Layered Aluminophosphate with a New 2D Network Topology. *J. Solid State Chem.*, **2005**, *178*, 2322-2331.

40. Maeda, K.; Kiyozumi, Y.; Mizukami, F. Characterization and Gas Adsorption Properties of Aluminum Methylphosphonates with Organically Lined Unidimensional Channels *J. Phys. Chem. B*, **1997**, *101*, 4402-4412.

41. Kanehashi, K.; Nemoto, T.; Saito, K. Through-Bond and Through-Space Connectivities of Amorphous Aluminophosphate by Two-Dimensional ^{27}Al–^{31}P Heteronuclear NMR. *J. Non-Cryst. Solids*, **2007**, *353*, 4227-4231.

42. Campomar, V. *PhD. Thesis*; Université P. et M. Curie, 1990.

43. Sutrisno, A.; Liu, L.; Xu, J.; Huang, Y. Natural Abundance Solid-State ^{67}Zn NMR Characterization of Microporous Zinc Phosphites and Zinc Phosphates at Ultrahigh Magnetic Field. *Phys. Chem. Chem. Phys.*, **2011**, *13*, 16606-16617.

44. Ashbrook, S. E.; Dawson, D. M.; Seymour, V. R. Recent Developments in Solid-State NMR Spectroscopy of Crystalline Microporous Materials. *Phys. Chem. Chem. Phys.*, **2014**, *16*, 8223-8242.

45. Cuny, J.; Messaoudi, S.; Alonzo, V.; Furet, E.; Halet, J.-F.; Le Fur, E.; Ashbrook, S. E.; Pickard, C. J.; Gautier, R.; Le Polles, L. DFT Calculations of Quadrupolar Solid-State NMR Properties: Some Examples in Solid-State Inorganic Chemistry. *J. Comput. Chem.*, **2008**, *29*, 2279-2287.

46. Charpentier, T. The PAW/GIPAW Approach for Computing NMR Parameters: A New Dimension Added to NMR Study of Solids. *Solid State Nucl. Magn. Reson.*, **2011**, *40*, 1-20.

47. Bonhomme, C.; Gervais, C.; Babonneau, F.; Coelho, C.; Pourpoint, F.; Azaïs, T.; Ashbrook, S. E.; Griffin, J. M.; Yates, J. R.; Mauri, F.; Pickard, C. J. First-Principles Calculation of NMR Parameters Using the Gauge Including Projector Augmented Wave Method: A Chemist's Point of View. *Chem. Rev.*, **2012**, *112*, 5733-5779.

48. Ashbrook S. E. and D. M. Dawson, Exploiting Periodic First-Principles Calculations in NMR Spectroscopy of Disordered Solids. *Acc. Chem. Res.*, **2013**, *46*, 1964-1974.

49. Sneddon, S.; Dawson, D. M.; Pickard, C. J.; Ashbrook, S. E. Calculating NMR Parameters in Aluminophosphates: Evaluation of Dispersion Correction Schemes. *Phys. Chem. Chem. Phys.*, **2014**, *16*, 2660-2673.

50. Clark, S. J.; Segall, M. D.; Pickard, C. J.; Hasnip, P. J.; Probert, M. J.; Refson, K.; Payne, M. C. First Principles Methods Using CASTEP. *Z. Kristallogr.*, **2005**, *220*, 567-570.

51. Pickard, C. J.; Mauri, F. All-Electron Magnetic Response with Pseudopotentials: NMR Chemical Shifts. *Phys. Rev. B*, 2001, **63**, 245101.

52. Wei, Y.; Tian, Z.; Gies, H.; Xu, R.; Ma, H.; Pei, R.; Zhang, W.; Xu, Y.; Wang, L.; Li, K.; Wang, B.; Wen, G.; Lin, L. Ionothermal Synthesis of an Aluminophosphate Molecular

Sieve with 20-Ring Pore Openings. *Angew. Chem. Int. Ed.*, **2010**, *49*, 5367 –5370.

53. Kihara, K.; Matsui, M. Molecular Dynamics Study of Structural Changes in Berlinite. *Phys. Chem. Mineral.*, **1999**, *26*, 601-614.

54. Martinez, J. D.; McCusker, L. B.; Baerlocher, C. Characterization and Structural Analysis of Differently Prepared Samples of Dehydrated VPI-5. *Micropor. Mesopor. Mater.*, **2000**, *34*, 99-113.

55. Griffin, J. M.; Berry, A. J.; Frost, D. J.; Wimperis, S.; Ashbrook, S. E. Water in the Earth's Mantle: a Solid-State NMR Study of Hydrous Wadsleyite. *Chem. Sci.*, **2013**, *4*, 1523-1538.

56. MacKenzie, K. J. D.; Smith, M. E. *Multinuclear Solid-State NMR of Inorganic Materials*; Elsevier Science Ltd, Oxford, UK, 2002.

57. Frisch, M. J.; Trucks, G. W. ; Schlegel, H. B.; Scuseria, G. E.; Robb, M. A.; Cheeseman, J. R.; Montgomery, J. A.; Vreven, T.; Kudin, K. N.; Burant, J. C. *et al*. GAUSSIAN03 revision D.01, Gaussian, Inc., Wallingford, CT, 2004.

58. Jensen, F. Basis Set Convergence of Nuclear Magnetic Shielding Constants Calculated by Density Functional Methods. *J. Chem. Theor. Comput.*, **2008**, *4*, 719-727.

59. Perdew, J. P.; Burke, K.; Ernzerhof, M. Generalized Gradient Approximation Made Simple. *Phys. Rev. Lett.*, **1996**, *77*, 3865-3868.

60. Yates, J. R.; Pickard, C. J.; Mauri, F. Calculation of NMR Chemical Shifts for Extended Systems Using Ultrasoft Pseudopotentials. *Phys. Rev. B* **2007**, 76, 024401.

61. MATLAB and Statistics Toolbox Release 2011b, The MathWorks, Inc., Natick, MA.

62. Graetsch, H. A. Hexagonal High-Temperature Form of Aluminium Phosphate Tridymite from X-ray Powder Data. *Acta Crystallogr.*, **2001**, *C57*, 665-667.

63. Ikeda, T.; Miyazawa, K.; Izumi, F.; Huang, Q.; Santoro, A. Structural Study of the Aluminophosphate $AlPO_4$-5 by Neutron Powder Diffraction. *J. Phys. Chem. Solids*, **1999**, *60*,

1531-1535.

64. Richardson, J. W.; Pluth, J. J; Smith, J. V. Rietveld Profile Analysis of Calcined $AlPO_4$-11 Using Pulsed Neutron Powder Diffraction. *Acta Crystallogr.*, **1988**, *B44*, 367-373.

65. Ghose, S.; Tsang, T. Structural Dependence of Quadrupole Coupling Constant e^2qQ/h for ^{27}Al and Crystal Field Parameter D for Fe^{3+} in Aluminosilicates. *Am. Mineral.*, **1973**, *58*, 748.

66. Zemann, J. Elektrostatische Energien von AB_5-Komplexen. *Z. Anorg. Allg. Chem.*, **1963**, *324*, 241-249.

67. Robinson, K.; Gibbs, G. V.; Ribbe, P. H. Quadratic Elongation: A Quantitative Measure of Distortion in Coordination Polyhedra. *Science*, **1971**, *172*, 567-570.

68. Kirkpatrick, R. J.; Brow, R. K. Nuclear Magnetic Resonance Investigation of the Structures of Phosphate and Phosphate-Containing Glasses: a Review. *Solid State Nucl. Magn. Reson.*, **1995**, *5*, 9-21.

69. Pichot, E.; Emery, J.; Quarton, M.; Dacheux, N.; Brandel, V.; Genet, M. Correlation between ^{31}P NMR and X-Ray Diffraction Data in the Refinement of the Atomic Positionf of the Thorium Phosphate-Diphosphate Crystal Structure. *Mater. Res. Bull.*, **2001**, *36*, 1347-1359.

70. Bussmann-Holder, A.; Dalal, N.; Fu., R; Migoni, R. High-Precision ^{31}P Chemical Shift Measurements on KH_2PO_4-Type Crystals.: Role of Electronic Instability in the Ferroelectric Transition Mechanism. *J. Phys.: Condens. Matter* **2001**, *13*, L231-L237.

71. Hartmann, P.; Jana, C.; Vogel, J.; Jäger, C. ^{31}P MAS and 2D Exchange NMR of Crystalline Silicon Phosphates. *Chem. Phys. Lett.*, **1996**, *258*, 107-112.

72 Coelho, C.; Azais, T.; Bonhomme-Coury, L.; Maquet, J.; Massiot, D.; Bonhomme, C. Application of the MAS-J-HMQC Experiment to a new Pair of Nuclei $\{^{29}Si,^{31}P\}$:$Si_5O(PO_4)_6$

and SiP_2O_7 Polymorphs. *J. Magn. Reson.*, **2006**, *179*, 114-119.

73 Krawietz, T. R.; Lin, P.; Lotterhos, K. E.; Torres, P. D.; Barich, D. H.; Clearfield, A.; Haw, J. F. Solid Phosphoric Acid Catalyst: a Multinuclear NMR and Theoretical Study. *J. Am. Chem. Soc.*, **1998**, *120*, 8502-8511.

74. Hansen, S. K.; Vestergaard, M.; Thøgersen, L.; Schiøtt, B., Nielsen, N. C.; Vosegaard, T. Lipid Dynamics Studied by Calculation of ^{31}P Solid-State NMR Spectra Using Ensembles from Molecular Dynamics Simulations. *J. Phys. Chem. B*, **2014**, *118*, 5119-5129.

Table 1. The systematic variation of P-O-Al bond angles ($\theta_{POAl(i)}$), in the series of model $[P(OAl(OH)_3)_4]^{3-}$ clusters (see Figure 2) studied here. The angles are expressed for the n^{th} member of the series, and the number of clusters in the series, N, is given.

Series	$\theta_{POAl(i)}$ (°)	N
1	$\theta_{POAl(1)} = \theta_{POAl(2)} = \theta_{POAl(3)} = \theta_{POAl(4)} = \langle \theta_{POAl} \rangle = 105 + 5n$	15
2	$\theta_{POAl(1)} = \theta_{POAl(2)} = 140$ $\theta_{POAl(3)} = 140 + 5n$ $\theta_{POAl(4)} = 140 - 5n$	7
3	$\theta_{POAl(1)} = \theta_{POAl(2)} = 140 + 5n$ $\theta_{POAl(3)} = \theta_{POAl(4)} = 140 - 5n$	7
4	$\theta_{POAl(1)} = 105 + 5n$ $\theta_{POAl(2)} = \theta_{POAl(3)} = \theta_{POAl(4)} = 140 + (140 - \theta_{POAl(1)})/3$	14
5	$\theta_{POAl(1)} = 150$ $\theta_{POAl(2)} = 105 + 5n$ $\theta_{POAl(3)} = \theta_{POAl(4)} = (410 - \theta_{POAl(2)})/2$	8
6	$\theta_{POAl(1)} = 120$ $\theta_{POAl(2)} = 175 - 5n$ $\theta_{POAl(3)} = \theta_{POAl(4)} = (440 - \theta_{POAl(2)})/2$	11
7	$\theta_{POAl(1)} = 105 + 5n$ $\theta_{POAl(2)} = \theta_{POAl(3)} = \theta_{POAl(4)} = 140$	15
8	all angles randomly generated,[a] $115.58 \leq \theta_{POAl(i)} \leq 167.41$	20

[a] For a full list of the randomly-generated angles, see the Supporting Information.

Table 2. The systematic variation of P-O bond lengths ($r_{PO(i)}$), in the series of model $[P(OAl(OH)_3)_4]^{3-}$ clusters (see Figure 2) studied here. The lengths are expressed for the n^{th} member of the series, and the number of clusters in the series, N, is given.

Series	$r_{PO(i)}$ / Å	N
9	$r_{PO(1)} = r_{PO(2)} = r_{PO(3)} = r_{PO(4)} = \langle r_{PO} \rangle = 1.44 + 0.01n$	14
10	$r_{PO(1)} = r_{PO(2)} = 1.52$ $r_{PO(3)} = 1.52 + 0.01n$ $r_{PO(4)} = 1.52 - 0.01n$	5
11	$r_{PO(1)} = r_{PO(2)} = 1.52 + 0.01n$ $r_{PO(3)} = r_{PO(4)} = 1.52 - 0.01n$	5
12	$r_{PO(i)} = 1.47 + 0.01n$ $r_{PO(2)} = r_{PO(3)} = r_{PO(4)} = 1.52$	9
13	all lengths randomly generated,[a] $1.45 \leq r_{PO(i)} \leq 1.57$	20

[a] For a full list of the randomly-generated lengths, see the Supporting Information.

Table 3. Summary of the distortion parameters used in this work. For full definitions, see the Supporting Information. In the formula column, the relevant structural parameter (bond length or angle) is denoted x, with $\langle x \rangle$ and x_0 denoting the mean and ideal (as defined in the Supporting Information) values of x, respectively.

Structural Distortion	Parameter	Formula[a]
deviation from mean bond length or angle	standard deviation	$\sigma(x) = \frac{1}{\sqrt{n}}\sqrt{\sum_{i=1}^{n}\left(x_i - \langle x \rangle\right)^2}$
	deviation	$\Delta(x) = \frac{1}{n}\sum_{i=1}^{n}\left(\frac{x_i - \langle x \rangle}{\langle x \rangle}\right)^2$
deviation from ideal tetrahedral bond lengths	longitudinal strain	$\left\|\alpha\right\| = \sum_{i=1}^{n}\left\|\ln\left(\frac{x_i}{x_0}\right)\right\|$
deviation from ideal tetrahedral bond angles	shear strain	$\left\|\Psi\right\| = \sum_{i=1}^{n}\left\|\tan\left(x_i - x_0\right)\right\|$
displacement of the central P atom from the centre of a PO_4 tetrahedron	displacement	$\mathbf{r}_{PO} = \sum_{i=1}^{n}\mathbf{r}_{PO(i)}$

[a] For the displacement parameter, $\mathbf{r}_{PO}$, $r_{PO(i)}$ denotes the i^{th} P-O bond vector (note the use of bold typeface for the displacement and regular typeface for the bond vectors).

Figure Captions

Figure 1. A plot of published experimental ^{31}P δ_{iso} against $\langle\theta_{POT'}\rangle$ (T′ = Al, Si, Ga or Zn) measured experimentally by Bragg diffraction for a range of AlPOs, SAPOs, GaPOs and other metallophosphates (MAPOs), for which the Müller relationship was used to assign the resonances. The relationships published by Müller *et al.*[12] and Kanehashi *et al.*[41] are indicated. The broken lines indicate the lines of best fit for the datasets (the line of best fit for the dense phases is the relationship of Müller *et al.*).

Figure 2. A $[P(OAl(OH)_3)_4]^{3-}$ cluster (series 1, n = 7) used as an analogue of the local environment of P in an AlPO framework.

Figure 3. (a and b) Plots of calculated ^{31}P σ_{iso} against $\langle\theta_{POAl}\rangle$ for the series of model $[P(OAl(OH)_3)_4]^{3-}$ clusters detailed in Table 1. (a) Series 1, 7 and 8 and (b) series 2, 3, 4, 5, and 6. In (b), the data point for series 1, n = 7, is also shown for reference. (c-e) Plots of calculated ^{31}P σ_{iso} against (c) max(θ_{POAl}), (d) min(θ_{POAl}) and (e) $\sigma(\theta_{POAl})$ for series 8.

Figure 4. Plot of calculated ^{31}P σ_{iso} against (a and b) $\langle r_{PO}\rangle$ and (c) $\sigma(r_{PO})$ for the series of model $[P(OAl(OH)_3)_4]^{3-}$ clusters detailed in Table 2.

Figure 5. (a and b) Plots of calculated (by CASTEP) ^{31}P σ_{iso} for 42 calcined and dense $AlPO_4$ phases, detailed in the Supporting Information, as a function of (a) $\langle\theta_{POAl}\rangle$ and (b) $\langle r_{PO}\rangle$. The best fit linear (and, in (b), quadratic) functions are shown and the points arising from the structure of AlPO-5 determined by Ikeda *et al.*[63] (ICSD 88566) are highlighted in

orange. (c and d) Plots of (c) $\sigma_{iso}(\langle\theta_{POAl}\rangle,\langle r_{PO}\rangle)$ and (d) σ_{iso}(structure) against ^{31}P σ_{iso} calculated by CASTEP. The ideal 1:1 correspondence is indicated in grey and the point for P3 of AlPO-11 (ICSD 63664) is highlighted in orange.

Figure 6. (a) Experimental (14.1 T, 14 k Hz) and (b - d) simulated ^{31}P NMR spectra of calcined AlPO-14. Spectra were simulated using values for σ_{iso} obtained from (b) CASTEP calculations, (c) $\sigma_{iso}(\langle\theta_{POAl}\rangle,\langle r_{PO}\rangle)$ (Equation 9) and (d) σ_{iso}(structure) (Equation 10), where a value of σ_{ref} of 279.28 ppm was used in all cases. In all calculated parameters, the CASTEP-optimised structure of the material was used as the input.

Figure 1

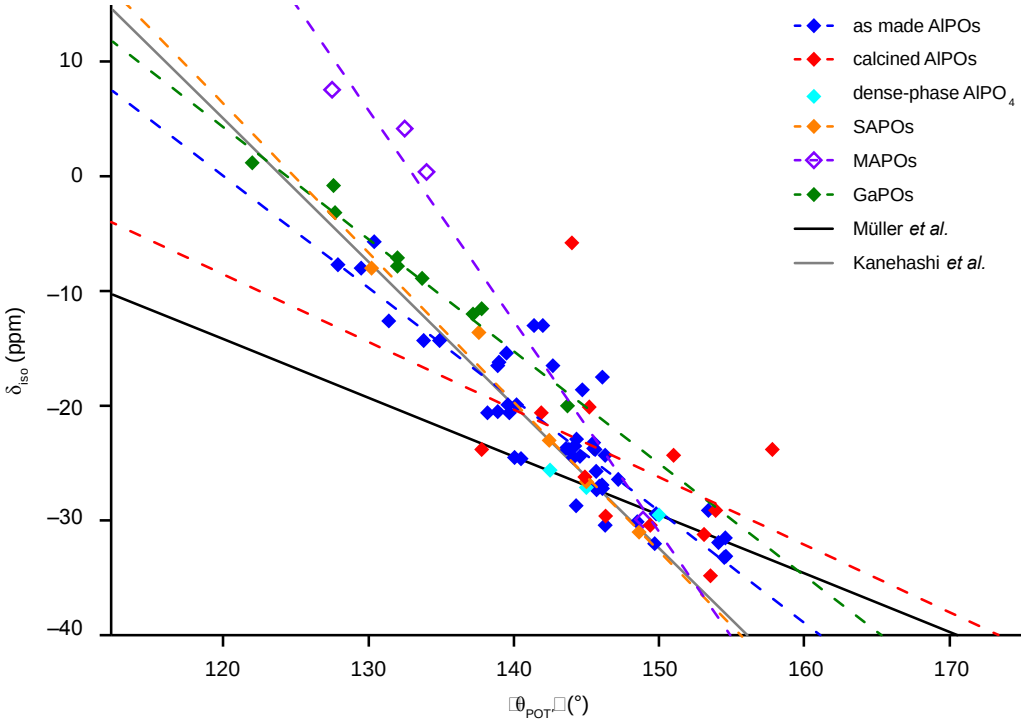

Figure 2

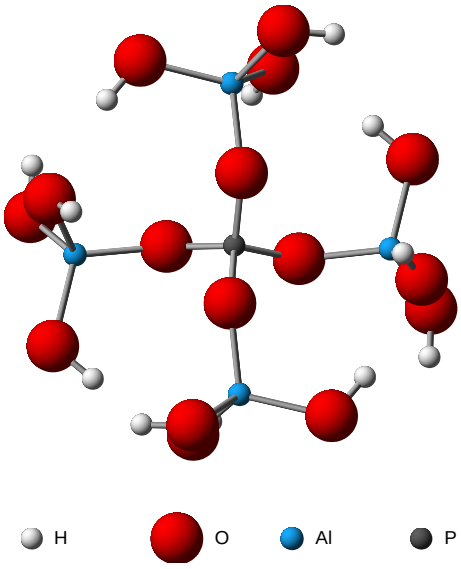

Figure 3

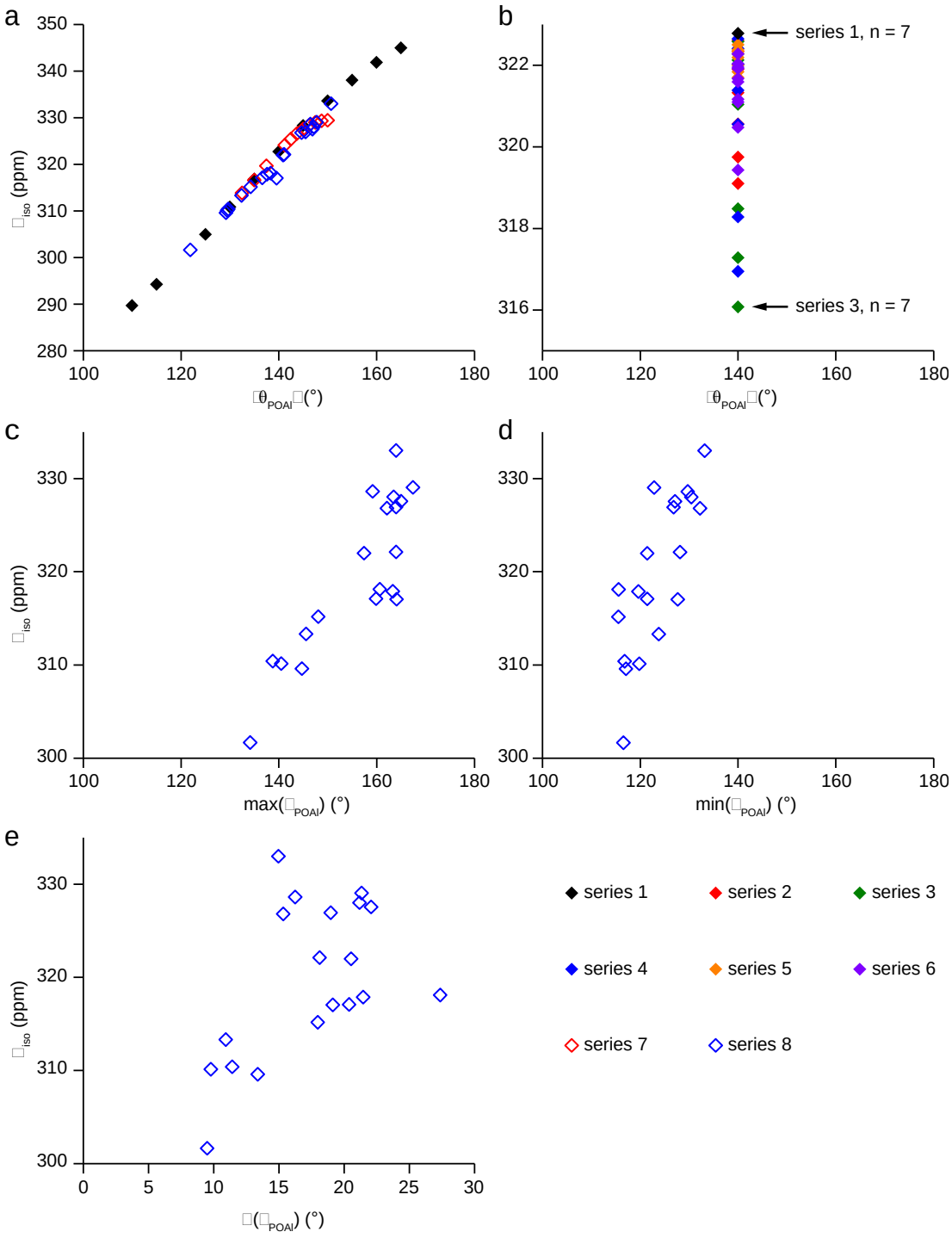
a
b
c
d
e
series 1, n = 7
series 3, n = 7
series 1
series 2
series 3
series 4
series 5
series 6
series 7
series 8

Figure 4

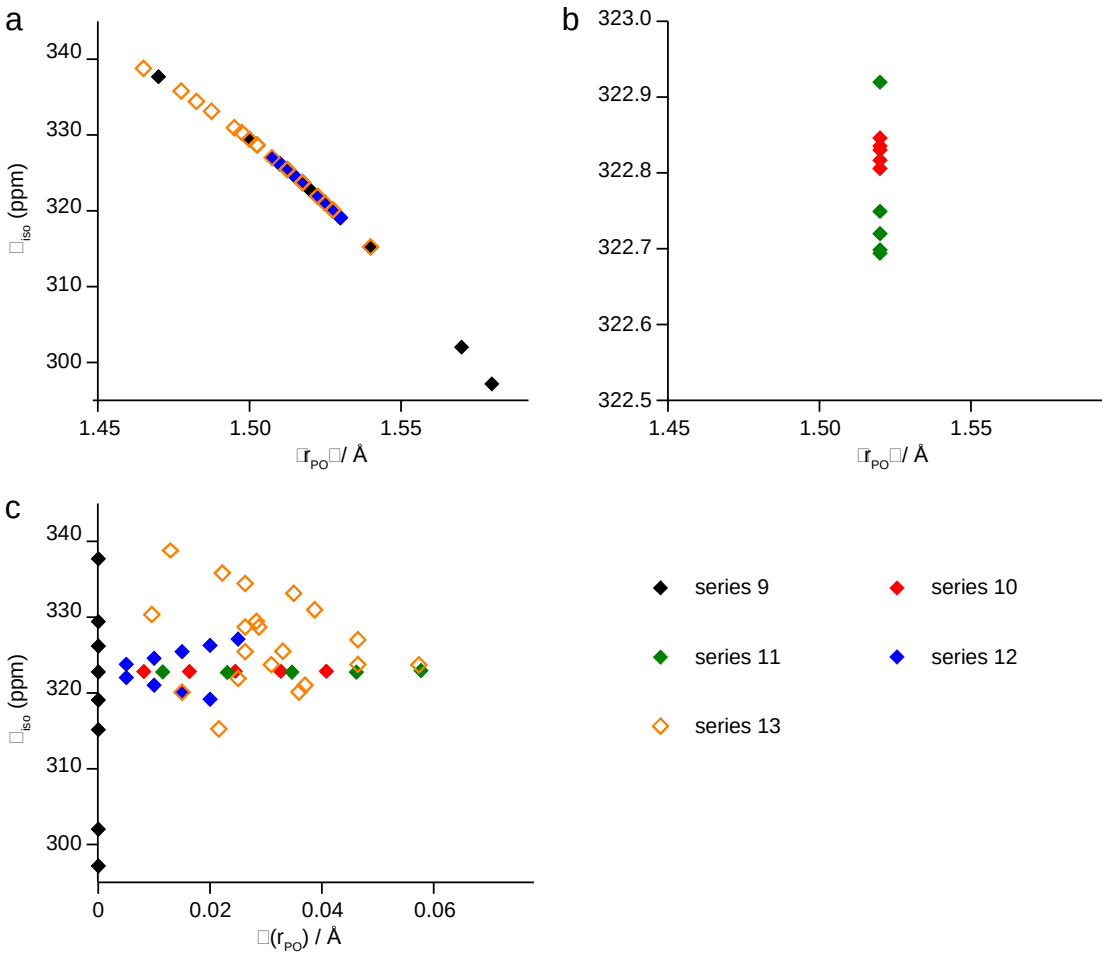
a
340
330
320
310
300
□iso (ppm)
1.45
1.50
1.55
□rPO□/ Å
b
323.0
322.9
322.8
322.7
322.6
322.5
1.45
1.50
1.55
□rPO□/ Å
c
340
330
320
310
300
□iso (ppm)
0
0.02
0.04
0.06
□(rPO) / Å
series 9
series 10
series 11
series 12
series 13

Figure 5

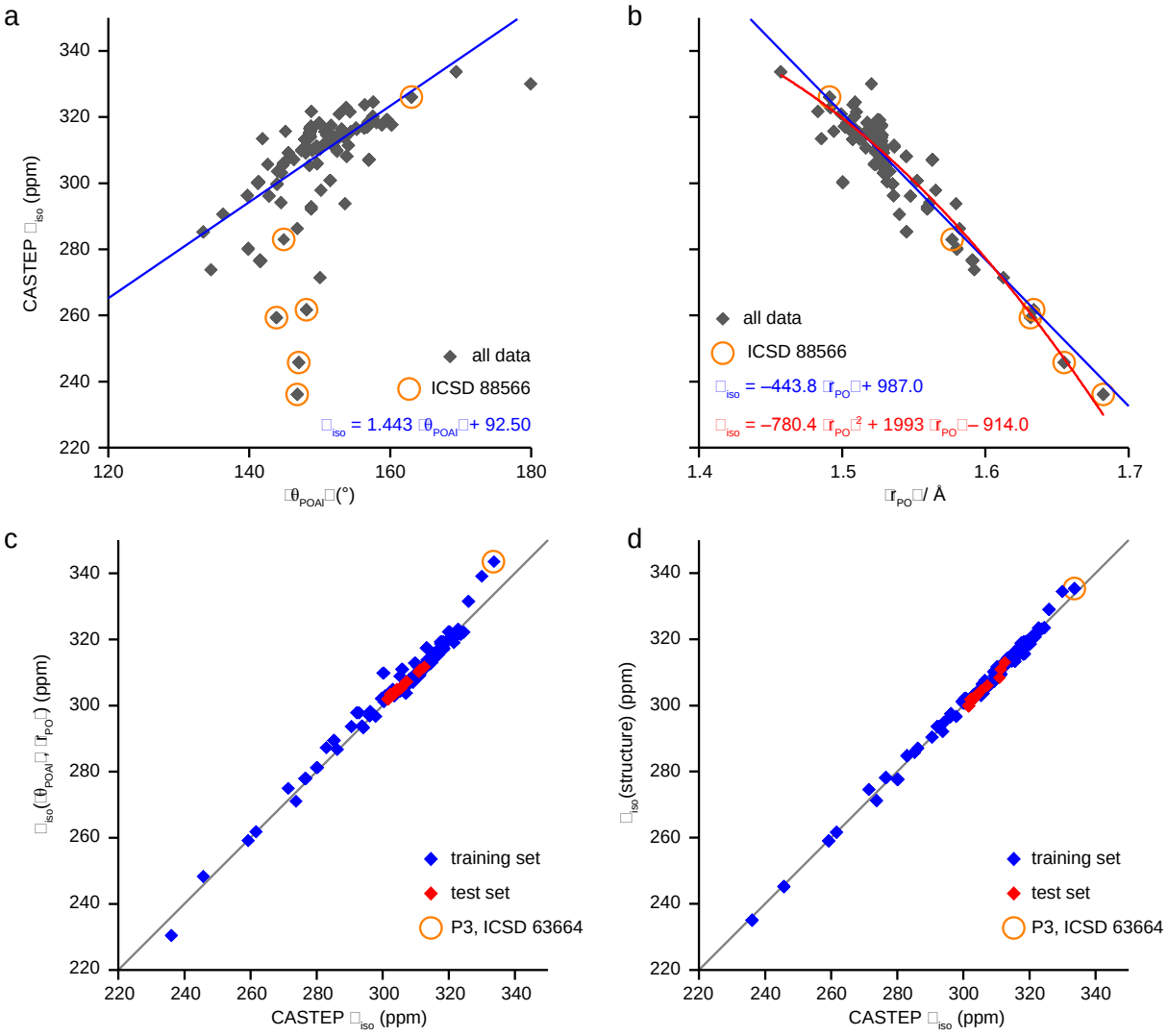
a
b
c
d
CASTEP □iso (ppm)
□θPOAl□(°)
all data
ICSD 88566
□iso = 1.443 □θPOAl□+ 92.50
□rPO□/ Å
□iso = –443.8 □rPO□+ 987.0
□iso = –780.4 □rPO□2 + 1993 □rPO□– 914.0
□iso(□θPOAl□, □rPO□) (ppm)
CASTEP □iso (ppm)
training set
test set
P3, ICSD 63664
□iso(structure) (ppm)

Figure 6

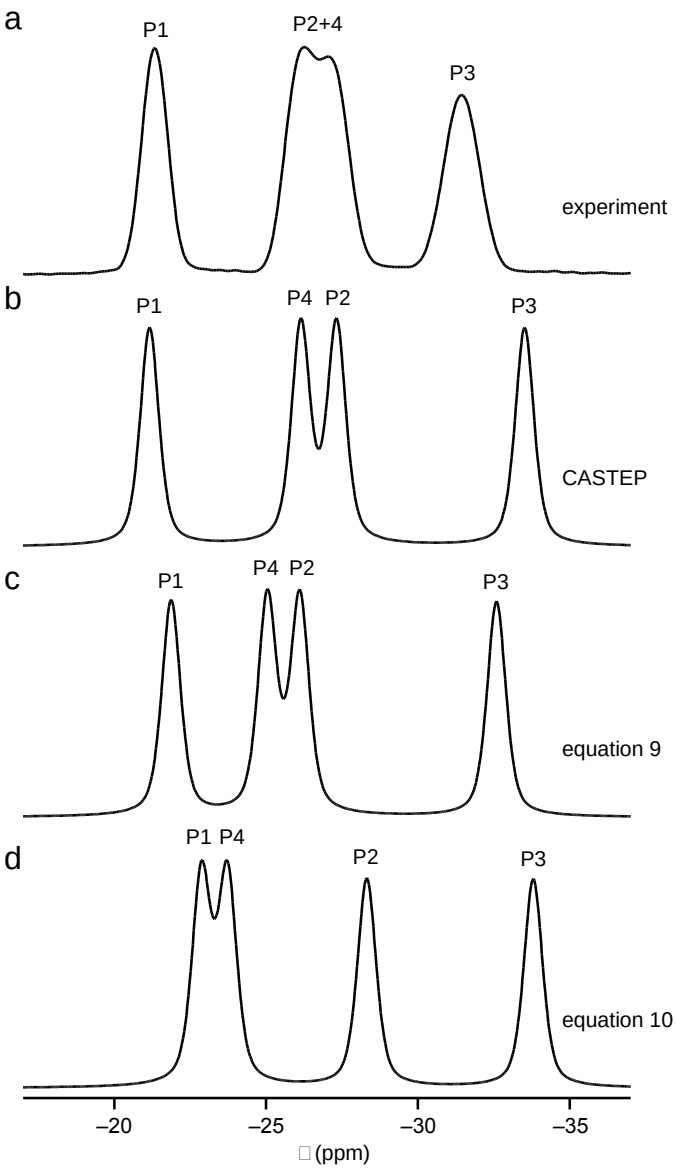
a
P1
P2+4
P3
experiment
b
P1
P4 P2
P3
CASTEP
c
P1
P4 P2
P3
equation 9
d
P1 P4
P2
P3
equation 10
–20
–25
–30
–35
(ppm)

TOC image